Polymer Testing 56 (2016) 277–286

Contents lists available at ScienceDirect

Polymer Testing

journal homepage: www.elsevier.com/locate/polytest

Material Properties

Gel P (VdF/HFP) / PVAc / lithium hexafluorophosphate composite electrolyte containing nano ZnO filler for lithium ion batteries application: Effect of nano filler concentration on structure, thermal stability and transport properties

Emad M. Masoud*, Mahmoud E. Hassan, Samar E. Wahdaan, Sahar R. Elsayed, Samar A. Elsayed

Chemistry Department, Faculty of Science, Benha University, 13518 Benha, Egypt

ARTICLE INFO

Article history:
Received 15 September 2016
Received in revised form
18 October 2016
Accepted 21 October 2016
Available online 22 October 2016

Keywords:
Polymer nano composites electrolytes
Ionic conductivity
Thermal stability
Lithium ion batteries

ABSTRACT

Nano ZnO filler incorporating gel co-polymer composites electrolytes membranes were prepared using a solution cast technique. All prepared membranes were characterized using different techniques such as X-ray diffraction (XRD), thermal analysis (TG, DSC), Fourier transform infra –red spectroscopy (FT-IR) and scanning electron microscopy (SEM). X-ray diffraction analysis showed the effect of lithium hexafluorophosphate ($LiPF_6$), poly vinyl acetate (PVAc) and nano zinc oxide (ZnO) on the crystalline structure of the polyvinylidene fluoride –co– hexafluoro propylene (PVdF-co-HFP) matrix containing ethylene carbonate (EC) and diethyl carbonate (DEC) as plasticizers. FT-IR analysis confirmed the good dissolution of the $LiPF_6$ salt and the good interaction of the nano ZnO filler with the co-polymer matrix. TG analysis showed the good thermal stability of the samples containing ZnO compared to the free one. Also, addition of nano ZnO filler enhanced the conductivity value of the co-polymer composites electrolytes. The sample containing 6 wt % of ZnO delivered the highest conductivity value of about $3.69 \times 10^{-4}\ \Omega^{-1}\ cm^{-1}$ at room temperature with a good thermal stability behavior ($T_d = 325\ ^\circ C$).

1. Introduction

Lithium ion batteries as a renewable energy source have been investigated in the past few decades. Their high energy density and efficiency makes them promising candidates for hybrid electronic/electric vehicles and portable electronics [1,2]. Lithium ion batteries can also be used for electrical energy storage from renewable energy sources generated by solar or wind. Nevertheless, lithium ion batteries are still associated with severe safety risks such as fire and explosion hazards owing to the use of flammable separators and liquid organic electrolytes [3]. Gel polymer electrolytes are receiving considerable attention as solid separators in lithium ion batteries [4,5] because of their simple process ability, feasibility to suit various cell geometries, cost competitiveness and safety [6] in addition to ionic conduction comparable to the one of the most used liquid electrolytes, mechanical flexibility, low density and stability [4,5,7]. According to the previous studies, different polymer matrixes having different chemical structures with various fillers have been studied [3–13]. PVdF and its co-polymers have been chosen as potentially interesting ones due to their promised properties [14] such as good solubility behavior in dispersed media, low glass transition temperature (T_g), low crystallinity nature, high dielectric constant, possibility of tuning the separator porosity degree and pore size, good contact at electrode/electrolyte interface and cathodic environment stability [7].

P[(VdF-HFP)] as an example has received a great attention because of its good thermal and electrochemical stability [15]. This copolymer has amorphous structure favoring the ionic conduction, and at the same time crystalline structure of PVdF works as a mechanical support [16]. previous literature works have showed encouraging results for P (VdF-HFP) - based polymer electrolytes with various types of dopant salts, such as lithium fluoro alkyl phosphate [17], lithium perchlorate [18] and lithium bis (tri fluoro methane sulfonyl) imide [19].

Ratner and Shriver [20] showed that the conduction of ions in the polymer electrolyte matrix is mainly due to the amorphous phase. Addition of nano fillers (metal oxides) were also used to improve the

* Corresponding author.
E-mail addresses: emad.youssef@fsc.bu.edu.eg, emad_masoud1981@yahoo.com (E.M. Masoud).

http://dx.doi.org/10.1016/j.polymertesting.2016.10.028
0142-9418/

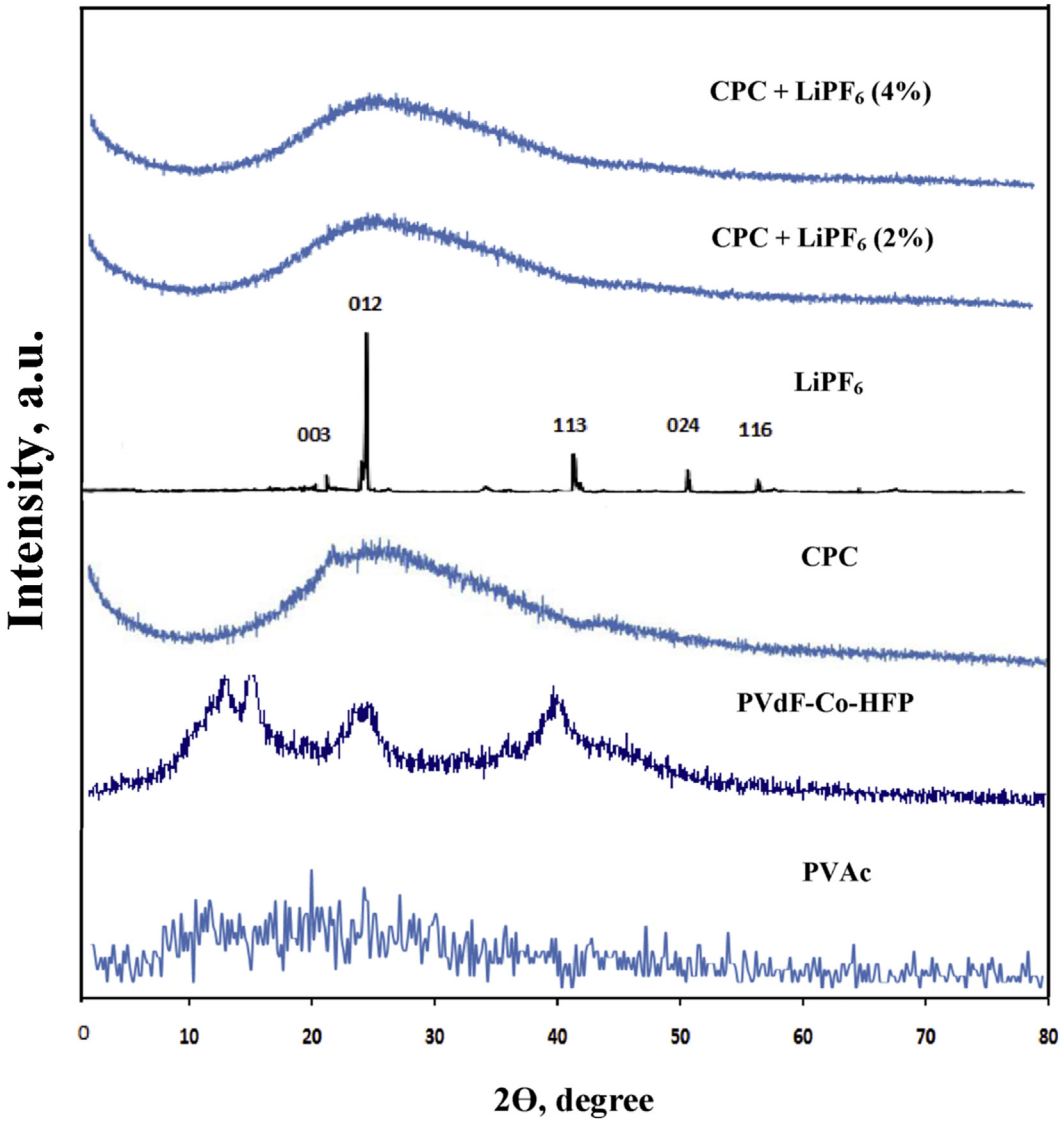

Fig. 1. X-ray diffraction patterns of PV_{AC}, PVdF-Co-HFP, CPC, $LiPF_6$ and CPC containing different concentrations of $LiPF_6$ (2, 4 wt %).

ionic conduction process in the gel polymer electrolytes [21,22].

In our present work, we try to prepare a membrane that can introduce the safety key as a gel polymer electrolyte. As the thermal stability is one of the most important properties supporting this safety, we will try to prepare a thermally stable electrolyte with good electrical properties using a mixture containing nano ZnO as a ceramic filler, lithium hexafluorophosphate ($LiPF_6$) as a salt and ethylene carbonate (EC) and diethyl carbonate (DEC) as plasticizers in presence of poly vinyl acetate (PVAc) as a good methodology in supporting the amorphous nature of the gel polymer electrolyte.

2. Experimental

Materials: pure reagent materials of zinc acetate [LOBA Chemie PVT.LTD., 98%], oxalic acid [Bio – Chem., 98%], P(VdF-co-HFP) (Sigma – Aldrich, 99.99%), PVAc (Sigma – Aldrich, 99.99%), Ethylene carbonate (Sigma – Aldrich, 99.99%), Diethyl carbonate (Sigma – Aldrich, 99.99%), Lithium hexafluorophosphate (Sigma – Aldrich, 99.99%).

2.1. Preparation of nano ZnO filler

0.045 mol of oxalic acid was dissolved in 300 ml distilled water. This solution was slowly added to a solution (300 ml) containing 0.03 mol of zinc acetate under stirring for 24 h. Zinc-oxalate precipitate was obtained and then filtered. The ppt. was washed with acetone several times to get rid of impurities and then dried at 120 °C for 30 min. Finally, the precursor was calcined for 30 min at 450 °C to get nano ZnO particles.

2.2. Preparation of co-polymer nano composites electrolytes

Firstly, the co-polymer composites electrolytes were prepared using a simple solvent casting technique. The two polymers (PVAc, PVdF-*co*-HFP) were first dissolved in a mixture of tetra hydro furan (THF) and di-methyl formamide (DMF) under heating (40 °C). The given amounts of plasticizers (EC: DEC, 1:1 in volume) were also added into the above polymer mixture. After that, $LiPF_6$ salt was added according to the following concentrations (wt. %):

$$[6.25\ (\mathrm{PVAc}) + 26.75 - \mathrm{x}(\mathrm{PVdF} - \mathrm{co} - \mathrm{HFP}) + 67(\mathrm{EC} - \mathrm{DEC}) + \mathrm{x}(\mathrm{LiPF_6}), \mathrm{x} = 0, 2, 4, 6, 8\ \mathrm{wt.\%}]$$

The obtained homogenous viscous slurry was poured into the Petri dish. The solvent was allowed firstly to evaporate slowly from

the composite at room temperature, and then was dried at 60 °C for 6 h. All prepared co-polymer composites electrolytes were mechanically stable expect those containing 6 and 8 wt % of $LiPF_6$ that showed a very low mechanical stable membranes. Therefore, those samples will be out of our characterization and measurements.

Secondly, the co-polymer nano composites electrolytes were prepared by nano filler ZnO addition to the optimized co-polymer composite electrolyte using the same method and according to the following concentrations (wt. %):

$$[6.25(PVAc) + 22.75(PVdF - co - HFP) + 67(EC - DEC) + 4(LiPF_6)]_{100-x} + x(ZnO), x = 0, 2, 4, 6, 8\ wt.\%]$$

The slurry was stirred continuously for 24 h to avoid the filler aggregation and to ensure the fine mixing. The obtained homogenous viscous slurry was poured into the Petri dish. The solvent evaporation was performed as mentioned above.

At last, the sample containing PVAc, PVdF-co-HFP, EC and DEC was denoted as CPC (Co-polymer composite); the sample containing PVAc, PVdF-co-HFP, EC, DEC and optimized $LiPF_6$ concentration was denoted as OCPCE (optimized co-polymer composite electrolyte); and the sample containing PVAc, PVdF-co-HFP, EC, DEC, optimized $LiPF_6$ concentration and optimized ZnO filler concentration was denoted as OCPNCE (optimized co-polymer nano composite electrolyte).

2.3. Characterizations

X-ray diffraction analysis was performed on a Diano (made by Diano Corporation, U.S.A.) with Cu-filtered CuKα radiation (λ = 1.5418 Å) energized at 45 kV, and 10 mA. The samples were measured at room temperature in the range from 2θ = 0° to 80°. Differential scanning calorimetry (DSC) and thermal gravimetric analysis (TG) were performed in air atmosphere with a constant heating rate of 10 °C/min. in a temperature range of 298–523 K (for co-polymer composites electrolytes) and 298–873 K (for co-polymer nano composites electrolytes) using Shimadzu DSC-60H. The Fourier transform infrared spectra of the samples were recorded in the range of 625–4000 cm^{-1} using a Brucker-FT-IR. Scanning electron microscopy was carried out with JOEL scanning electron microscopy (JSM-35CF). Ionic conductivity of the co-polymer nano composites electrolytes was estimated with the help of stainless steel blocking electrodes using a programmable automatic LCR bridge (Model RM 6306 Phillips Bridge) in various temperatures ranging from 298 to 388 K.

3. Results and discussion

3.1. Effect of $LiPF_6$ addition on CPC

3.1.1. X-ray analysis

X-ray diffraction patterns of PVAc, PVdF-co-HFP, $LiPF_6$, CPC and CPC containing different concentrations of $LiPF_6$ (2, 4 wt %) are displayed in Fig. 1. The humps observed for PVAc confirm its amorphous nature. The XRD pattern of the PVdF-co-HFP polymer confirmed its semi crystalline nature [23]. The absence of the characteristic crystalline peaks of PVdF-co-HFP in the CPC sample confirms the good effect of PVAc on the semi crystalline structure of PVdF-co-HFP. More notably, the sharp crystalline peaks of $LiPF_6$ disappeared in the samples of $LiPF_6$ containing CPC to retrieve the good dissolution behavior of the $LiPF_6$ in the PVdF-co-HFP matrix structure.

3.1.2. Differential scanning calorimetry (DSC) analysis

DSC thermograms of CPC and CPC containing different concentrations of $LiPF_6$ (2, 4 wt %) are shown in Fig. 2. The crystallinity relative percentage (X_c) was calculated using the equation [24]:

$$X_c = \Delta H_c / \Delta H_p \quad (1)$$

where ΔH_p equals to 104.7 J/g which is the heat enthalpy of 100% crystalline PVdF [25], and ΔH_c is the heat enthalpy of CPC and CPC containing different concentrations of $LiPF_6$. The calculated relative crystallinity (X_C) and the data obtained from DSC thermograms are shown in Table 1. The melting temperature (T_m) of CPC decreases continuously by the addition of $LiPF_6$ to show that the sample

Table 1
Values of melting temperature (T_m), heat enthalpy of melting (ΔH_m) and crystallinity percent (X_c) of CPC and CPC containing different concentrations of $LiPF_6$ (2, 4 wt %).

Sample	T_m,°C	ΔH_m, J/g	X_c, %
CPC	161.94	4.44	4.24
CPC – $LiPF_6$ (2 wt %)	161.48	8.18	7.81
CPC – $LiPF_6$ (4 wt %)	160.98	7.10	6.78

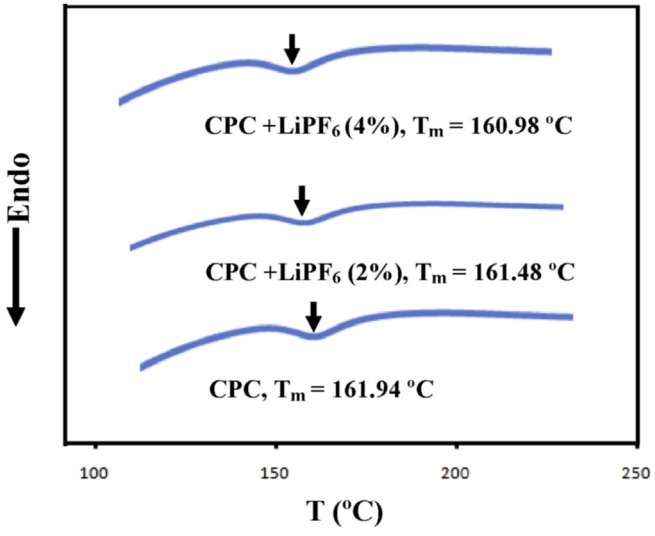

Fig. 2. Differential scanning calorimetry (DSC) of CPC and CPC containing different concentrations of $LiPF_6$ (2, 4 wt %).

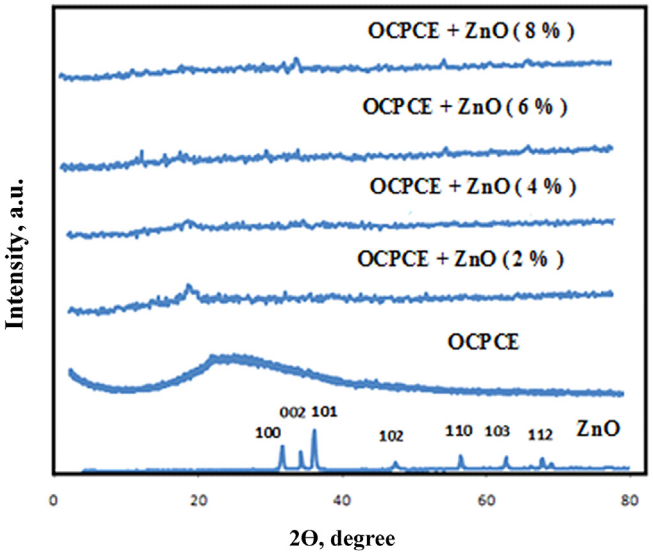

Fig. 3. X-ray diffraction patterns of ZnO, OCPCE and OCPCE containing different concentrations of ZnO (2, 4, 6, 8 wt %).

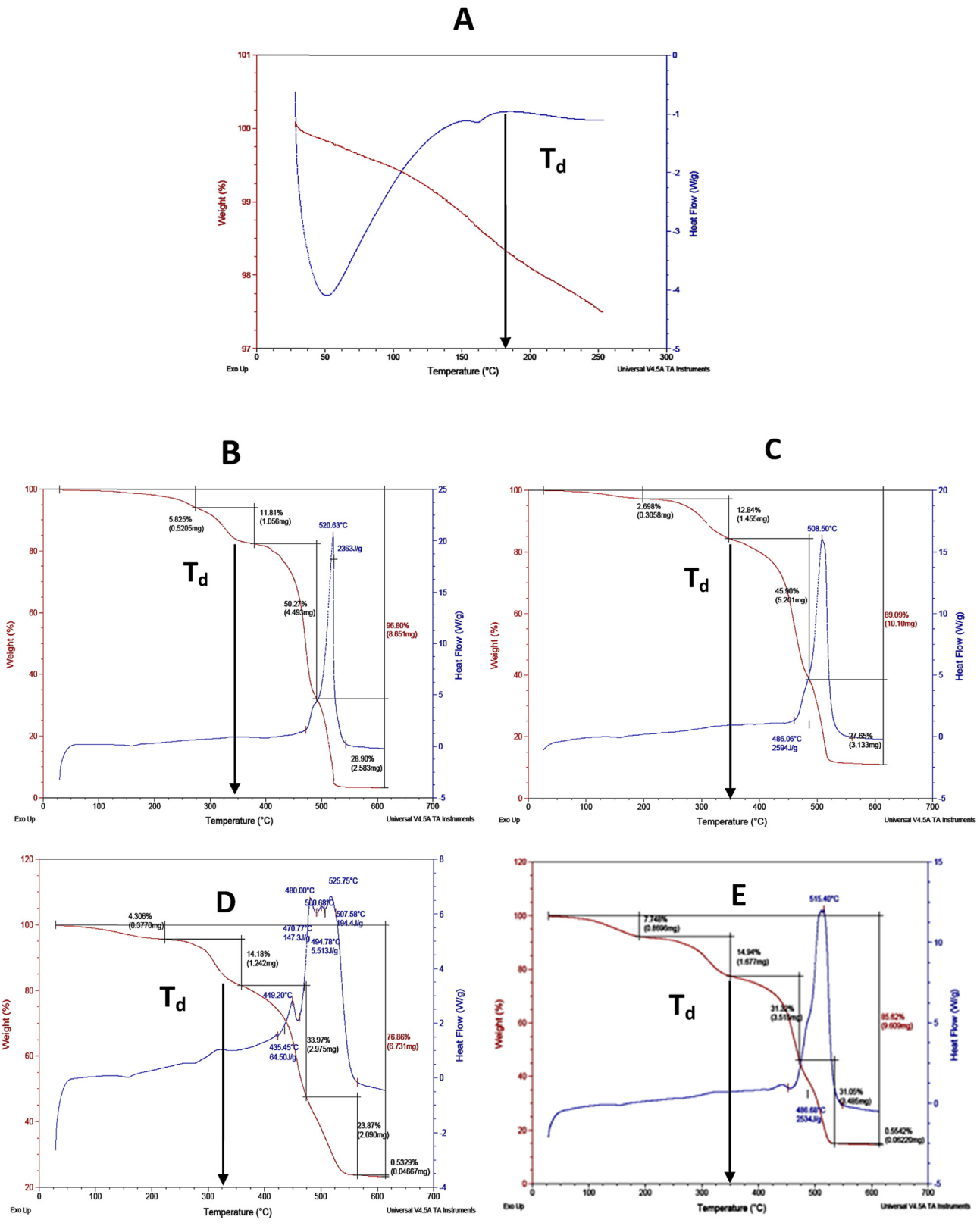

Fig. 4. Thermal analysis (TG-DSC) of OCPCE (A) and OCPCE containing different concentrations of ZnO: (B) 2 (C) 4 (D) 6 and (E) 8 wt%.

containing 4 wt % of $LiPF_6$ has the low melting temperature value ($T_m = 160.98\ ^\circ C$). On the other hand, the crystallinity relative percentage (X_C) increased in presence of $LiPF_6$ salt compared to the pure CPC sample, showing that the sample containing 4 wt% of $LiPF_6$ has also the low crystallinity value ($X_C = 6.78\%$).

3.2. *Effect of nano ZnO filler addition on OCPCE*

3.2.1. *X-ray analysis*

X-ray diffraction patterns of ZnO, OCPCE and OCPCE containing different concentrations of ZnO (2, 4, 6, and 8 wt %) are displayed in

Fig. 3. The ZnO pattern shows typical peaks characterized for ZnO [26] and a good consistence with JCPDS (NO. 361451). XRD line broadening was used to estimate the crystallite size of the powder according to Scherer formula [27]:

$$D = 0.9\lambda/\beta\cos\theta \quad (2)$$

Where λ is the wavelength of x-ray, θ is the Bragg angle and β is the full width half maximum in radians calculated using Gaussian fitting. The results showed an average crystalline size of about 8 nm.

Also, from the figure, we can observe the effect of nano ZnO filler addition on OCPCE sample as its broad hump was completely disappeared, confirming the destruction effect of the filler on the ordered arrangement of the co-polymer side chains, and hence an enhancement in the amorphous phase. This destruction effect may be due to Lewis acid - base interactions between the filler surface and the polar fluoride atom (F) of PVdF-co-HFP.

3.2.2. *Differential scanning calorimetry (DSC) and thermal gravimetric (TG) analyses*

DSC and TG thermograms of OCPCE and OCPCE containing different concentrations of ZnO (2, 4, 6, 8 wt %) are shown in Fig. 4. The crystallinity relative percentage (X_c) was also calculated using equation (1). The data obtained from DSC thermograms are shown in Table 2. The table showed that melting temperature (T_m) of OCPCE decreases by addition of ZnO (2 wt %) and then increases for the sample of 4 wt % of ZnO. After that, a continuous decrease was observed till 8 wt % of ZnO. The sample containing 8 wt % ZnO has the low value (T_m = 156.88 °C) compared to the others. The crystallinity relative percentage (X_C) values also showed an irregular trend, where the sample containing 6 wt % of ZnO has the low value (X_C = 8.77%).

To further show the effect of nano ZnO filler addition on the thermal decomposition of the OCPCE, thermal gravimetric (TG) analysis was also investigated, Fig. 4.

For the ZnO free sample, OCPCE, (Fig. 4A), the TG analysis was only performed till 250 °C, to exactly show the start of the sample decomposition, and to determine its accurate temperature value. After that, all the other samples were analyzed till 600 °C to approve the thermal stability in presence of nano ZnO filler.

It is observed from Fig. 4A that there is a preliminary weight loss in the temperature range of room temperature −150 °C. This can be attributed to the removal of moisture and/or the absorbance of water by the sample during the loading and the weight loss is in agreement with the endothermic peak observed in the DSC curve. The sample starts to melt at 160.98 °C (another endothermic peak was also observed, DSC curve). The determined total weight loss till melting temperature was about 1.5%. After that, the sample starts to decompose at 185 °C.

Table 2
Values of melting temperature (T_m), heat enthalpy of melting (ΔH_m), crystallinity percent (X_c), decomposition temperature (T_d) and AC-ionic conductivity (σ_{AC}) of OCPCE and OCPCE containing different concentrations of ZnO (2, 4, 6, 8 wt %).

Sample	T_m,°C	ΔH_m, J/g	X_c, %	T_d, °C	σ_{AC} ($ohm^{-1}.cm^{-1}$) at 298 K
OCPCE	160.98	7.10	6.78	185	1.00×10^{-6}
OCPCE - ZnO (2 wt %)	159.82	11.44	10.93	346	1.58×10^{-4}
OCPCE - ZnO (4 wt %)	160.00	11.74	11.21	350	1.58×10^{-5}
OCPCE - ZnO (6 wt %)	159.26	9.18	8.77	325	3.69×10^{-4}
OCPCE - ZnO (8 wt %)	156.88	12.65	12.08	345	1.00×10^{-5}

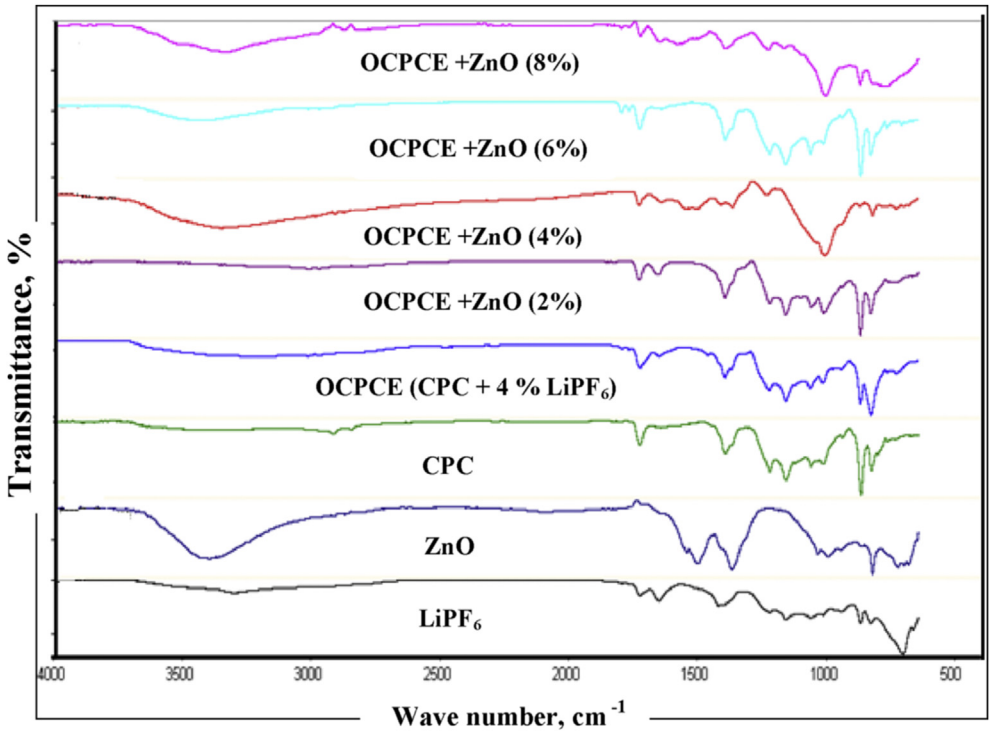

Fig. 5. FT-IR spectra of $LiPF_6$, ZnO, CPC, OCPCE and OCPCE containing different concentrations of ZnO (2, 4, 6, 8 wt %).

For all the other samples, the same behavior was observed with a temperature increase shift of all preliminary changes (removal water, melting) and decomposition, confirming the good thermal stability of all ZnO OCPCE samples. All values of decomposition temperatures (T_d) of all samples were shown in Table 2. It is obvious from the table that the OCPCE sample containing 4 wt % of ZnO has the highest value (350 °C) and that containing 6 wt % of ZnO has the lowest one (325 °C). The decomposition weight loss was mainly due to the degradation of the side chains of the polymers. This was confirmed by the exothermic peaks observed through the DSC curves. The different remaining weight percentage of all analyzed samples could be due to the presence of ZnO or due to the presence of –CF based back bones of the PVdF-co-HFP co-polymer [28].

3.3. FT-IR analysis

To explore the interactions between the polymers, salt and the filler, FT-IR spectra were investigated. Fig. 5 shows the FT-IR transmittance spectra of $LiPF_6$, ZnO, CPC, OCPCE and OCPCE containing different concentrations of ZnO (2, 4, 6, 8 wt %). The CPC

Table 3
FT-IR spectral bands assignment of CPC, OCPCE and OCPCE containing different ZnO concentrations.

Wave number (cm^{-1})	Band assignment					
	CPC	OCPCE	2 wt% ZnO	4 wt% ZnO	6 wt% ZnO	8 wt% ZnO
799	C-H wagging of PVAc	809	815	821	823	827
947	-CH bending of PVAc	954	946	946	946	–
1033	C-O stretching of PVAc	1039	1039	1039	1042	1042
1243	C-O–C stretching of PVAc	1249	1255	1258	1252	1248
1373	CH3 symmetric bending of PVAc	1381	1381	1374	1377	1377
1734	C=O stretching of PVAc	1745	1750	1755	1756	1756
2933	CH3 asymmetric stretching of PVAc	–	–	–	–	2941
763	Crystalline phase VdF unit of PVdF-co-HFP	765	766	766	766	766
1200	-CF2group of PVdF-co-HFP	1209	1213	1214	1199	1199
1390	CF2-deformation of PVdF-co-HFP	1399	1403	1403	1403	1403

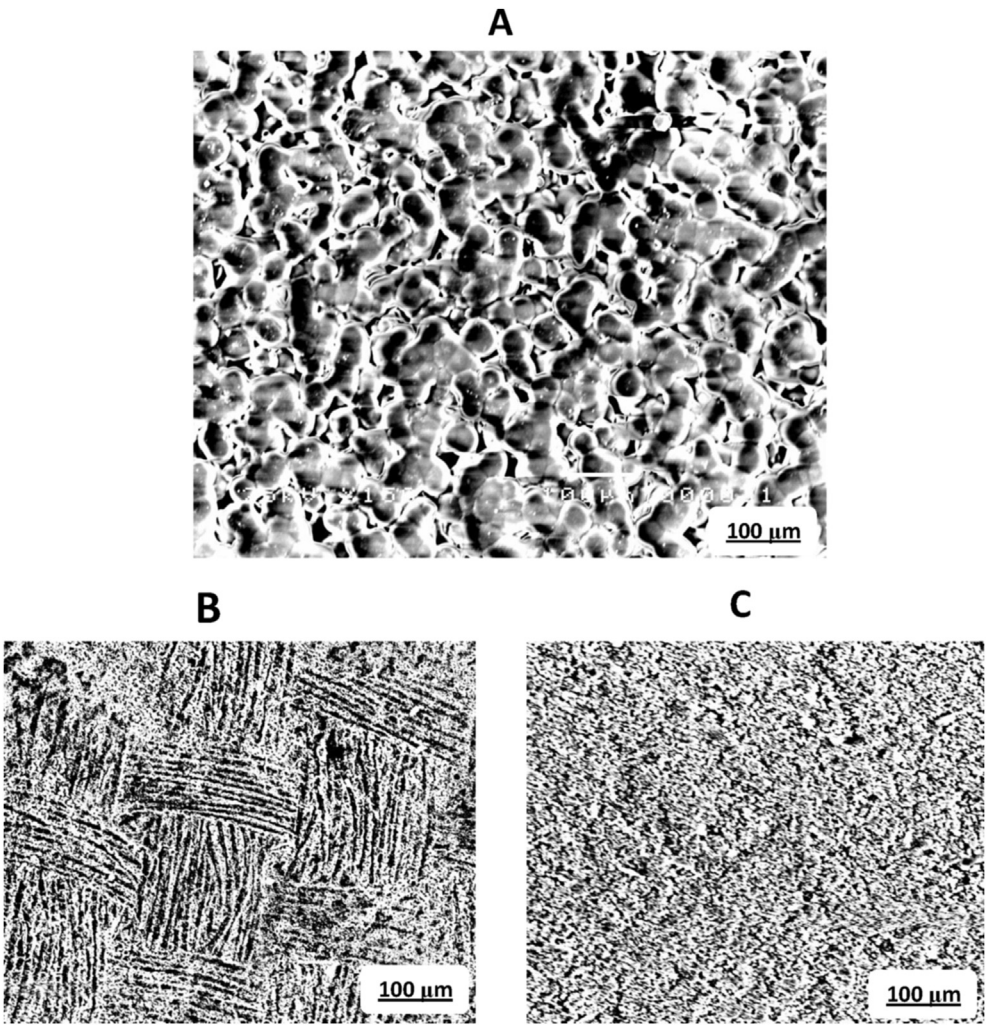

Fig. 6. SEM images of A) PVdF - co- HFP matrix; B) OCPCE and C) OCPCE containing 6 wt % of ZnO (OCPNCE).

sample showed different bands characteristic to PVAc or PVdF-co-HFP [26], Table 3. All frequency characteristics changes of OCPCE and OCPCE containing different ZnO concentrations are also shown in Table 3. The table showed that some bands of CPC were disappeared or shifted to higher or lower wave numbers in presence of the salt (OCPCE) and the different concentrations of ZnO filler, confirming the interactions between the CPC, salt and filler. Also, some peaks corresponding to $LiPF_6$ are not observed in the electrolytes, leading to the conclusion that $LiPF_6$ is dissolved in the co-polymer matrix. On the other hand, characteristic peak of ZnO filler appears at 1557 cm^{-1} [29] was shifted in some composites and disappeared in the other ones, to also confirm the interactions.

3.4. Scanning electron microscopy

To further study the effect of PVAc, $LiPF_6$ salt and nano ZnO filler on the co-polymer matrix morphology, SEM characterization was performed, Fig. 6 (A, B, C). As we can see, the pure PVdF-co-HFP matrix showed an obvious porous structure, Fig. 6(A). Also, the OCPCE sample showed less porous structure with different shape, reflecting the effect of $LiPF_6$ and PVAc on the porosity of the co-polymer matrix, Fig. 6(B). More notably, the OCPNCE sample showed homogeneous non porous matrix, confirming the ability of nano ZnO to fill the pores of the co-polymer matrix with a homogeneous distribution, Fig. 6(C).

3.5. Electrical properties

The temperature dependence of electrical conductivity (AC) of OCPCE and OCPCE containing different concentrations of ZnO (2, 4, 6, 8 wt %) is investigated in a temperature range of 298–388 K and illustrated in Fig. 7. The figure shows that the AC-ionic conductivity of composites increases in general with temperature increase. According to the linear behavior of curves, activation energy (E_a) values can be calculated using Arrhenius model, $\sigma = \sigma_0 \exp(-E_a/RT)$, where R, T, σ and σ_0 are gas constant, temperature, the AC-ionic conductivity and the pre-exponential factor, respectively. The values of activation energy change with filler content to have a minimum value of 0.08 eV for the OCPCE containing 6 wt % of ZnO, and a maximum one of 0.16 eV for the OCPCE containing 8 wt % of ZnO, Fig. 8. The values variation of AC-ionic conductivity at room temperature with the filler content can also be seen, Fig. 7. The figure showed that the AC-ionic conductivity at room temperature has the following order: σ_{Ac}(OCPCE, 6 wt % ZnO) > σ_{Ac}(OCPCE, 2 wt % ZnO) > σ_{Ac}(OCPCE, 4 wt % ZnO) > σ_{Ac} (OCPCE, 8 wt % ZnO) > σ_{Ac}(OCPCE). All values of room temperature AC- conductivity are shown in Table 2. In general, the filler samples showed high conductivity values compared to the free one. This can be interpreted by Croce et al. [30]. They suggested that filler can help to increase the conductivity by providing special Li^+ conducting pathways at the filler surface region through the Lewis acid −base interactions among different species in these filler samples.

The temperature dependence of dielectric constant (ε') and loss (ε") at a frequency of 100 Hz for OCPCE and OCPCE containing different concentrations of ZnO is shown in Fig. 9A and B. In general, it can be seen that ε' and ε" increases as temperature increases. The increase of dielectric constant with temperature can be ascribed to two mechanisms. Polymer nano composite electrolyte viscosity decrease is the first one [31] and the second is the dissolution of crystalline and semi-crystalline phases into the

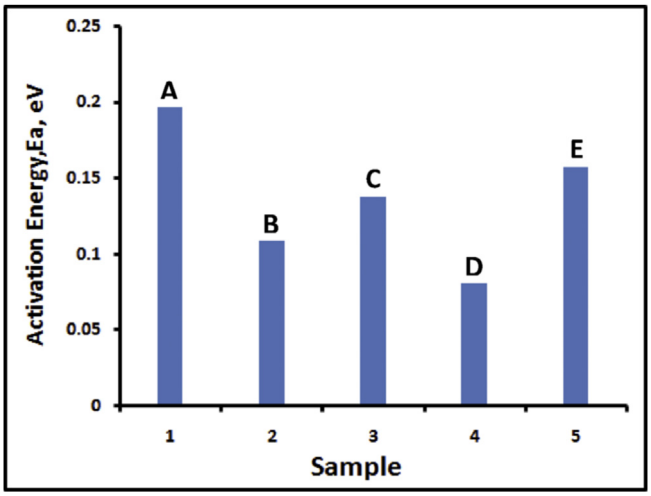

Fig. 8. Activation energy (E_a) values of A) OCPCE; B) OCPCE + 2 wt % ZnO; C) OCPCE + 4 wt % ZnO; D) OCPCE + 6 wt % ZnO; E) OCPCE + 8 wt% ZnO.

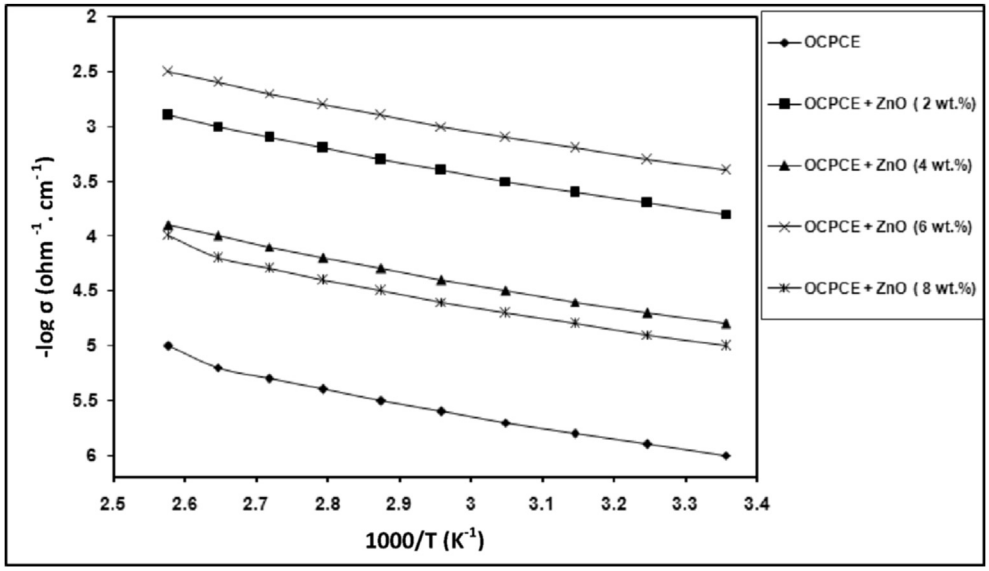

Fig. 7. Temperature dependent AC-ionic conductivity (100 Hz) plots of OCPCE and OCPCE containing different concentrations of ZnO (2, 4, 6, 8 wt %).

amorphous phase [32]. On the other hand, the dielectric loss increase with temperature increasing is due to the relaxation of the dipoles in co-operation with the drop in the relaxation time. Such high dielectric constant and loss values can be attributed to the high ionic conductivity that can be related to the presence of ZnO nano particles and its good distribution within the co - polymer matrix and also due to the good interactions between the Lewis acidic sites on the surface of those particles and the ions of lithium hexa fluoro phosphate [33]. More notably, the values of dielectric constant (ε′) and loss (ε") of all composites comes in the same order of AC- conductivity, where the OCPCE containing 6 wt % of ZnO showed the highest values (2×10^3 and 19450 for dielectric constant (ε′) and loss (ε") at room temperature and 100 Hz, respectively).

Fig. 10 shows a complex impedance plot of OCPNCE (OCPCE containing 6 wt % of ZnO), the optimized sample of high electrical properties. An impedance spectrum containing a semi – circle and an inclined straight line was observed. The semicircle part can be attributed to the conduction process and the linear one is due to the blocking electrode effect and the capacitance at the electrode –

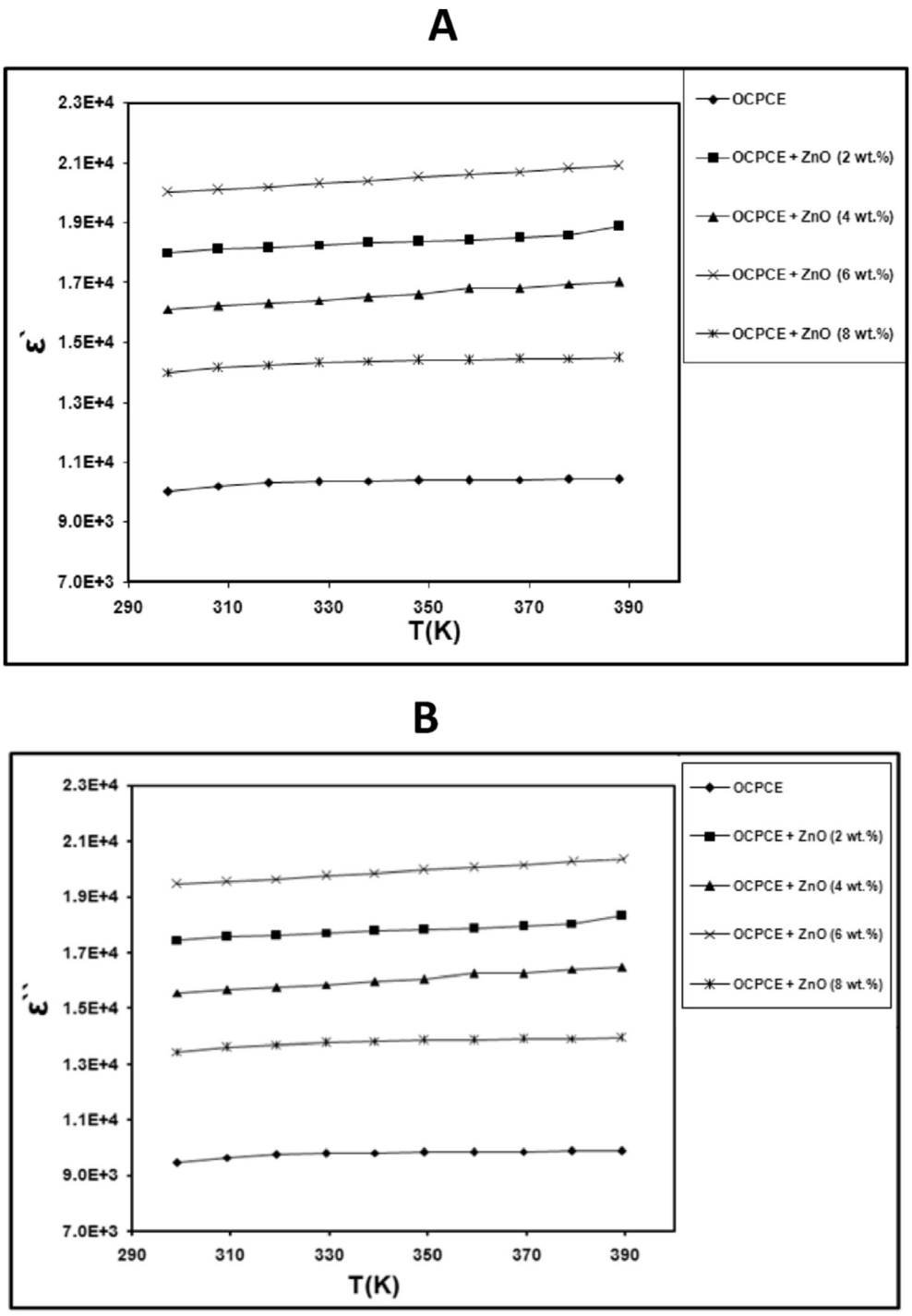

Fig. 9. Temperature dependence of (A) dielectric constant and (B) dielectric loss plots of OCPCE and OCPCE containing different concentrations of ZnO (2, 4, 6, 8 wt %) at a frequency of 100 Hz.

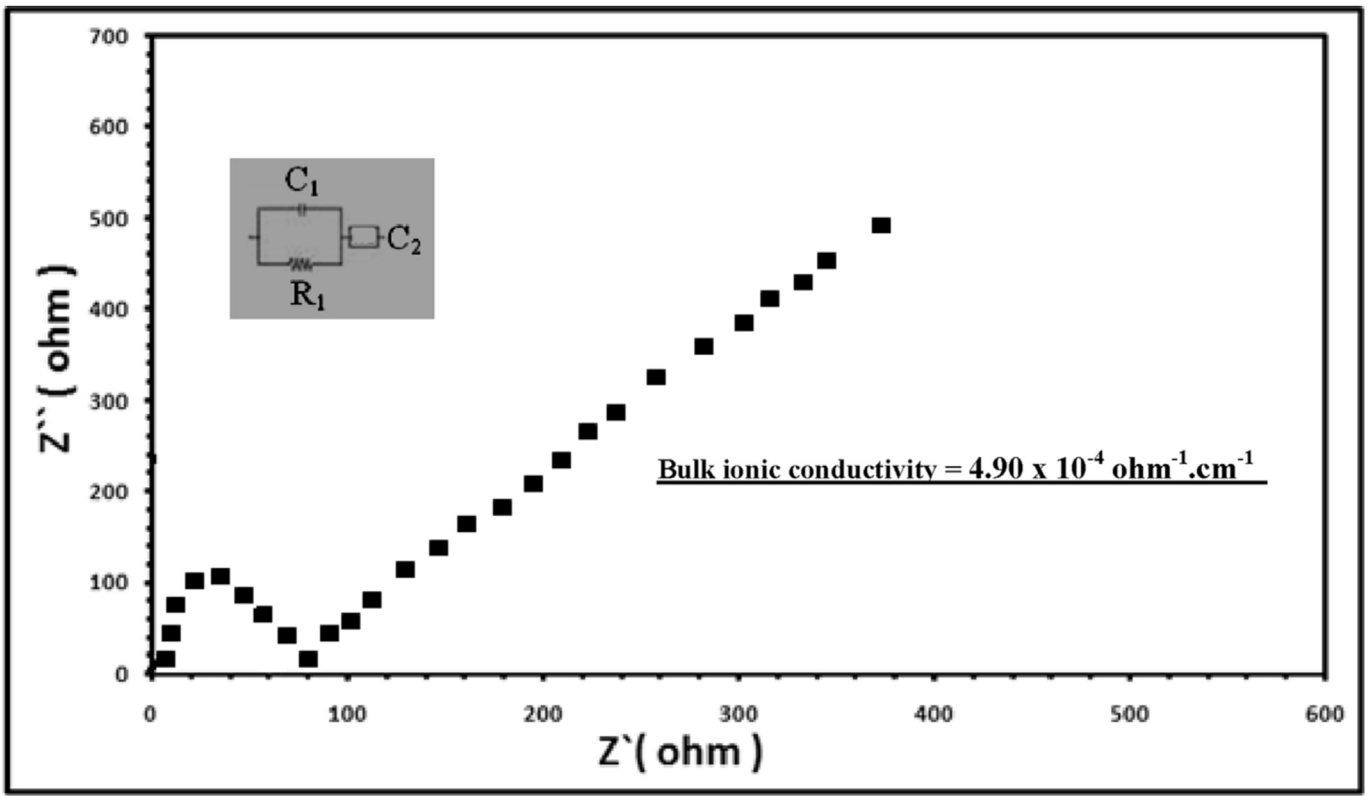

Fig. 10. Complex impedance of OCPCE containing 6 wt % of ZnO (OCPNCE) at room temperature (298 K).

electrolyte interface [34,35]. This blocking electrode results in a charge polarization in the copolymer matrix bulk and as a result, the electrical double layer at each interface will lead to increase the impedance against ion motion with frequency decreasing. The bulk ionic conductivity value was also calculated to equal $4.9 \times 10^{-4}\ \Omega^{-1}\ cm^{-1}$ at room temperature. The equivalent circuit was determined from the complex impedance spectrum and shown in Fig. 10. Where R1 is the bulk resistance of the electrolyte, C_1 is the bulk capacity of the electrolyte and C_2 is a capacity of bulk electrode − electrolyte interface.

4. Conclusions

Gel co-polymer composites electrolytes and gel co-polymer nano composites electrolytes were prepared using solution cast technique. Each of composites electrolytes was characterized using X-ray diffraction (XRD), thermal analysis (TG, DSC), Fourier transform infra red spectroscopy (FT-IR) and scanning electron microscopy (SEM). The effect of PVAc, $LiPF_6$ and nano ZnO on the crystalline structure and thermal stability behavior of all investigated composite electrolytes was confirmed. The optimized sample containing 4 wt % of $LiPF_6$ salt showed the less crystalline structure ($X_c = 6.78\%$) compared to the other composites electrolytes ones. The sample containing 6 wt % of ZnO showed the less crystalline structure ($X_c = 8.77\%$) and the highest conductivity value at room temperature ($3.69 \times 10^{-4}\ \Omega^{-1}\ cm^{-1}$) compared to the other nano composites electrolytes. The AC-ionic conductivity, at room temperature and 100 Hz, has the following order: σ_{Ac} (OCPCE, 6 wt % ZnO) > σ_{Ac} (OCPCE, 2 wt % ZnO) > σ_{Ac} (OCPCE, 4 wt % ZnO) > σ_{Ac} (OCPCE, 8 wt % ZnO) > σ_{Ac} (OCPCE). The same sample showed high values of dielectric constant and loss at room temperature (2×10^3 and 19450 for dielectric constant (ε') and loss (ε") at 100 Hz, respectively), demonstrating the high ion orientation within the gel copolymer composite electrolyte. The value of bulk ionic conductivity was also calculated to equal $4.90 \times 10^{-4}\ \Omega^{-1}\ cm^{-1}$ at room temperature. More importantly, the OCPNCE sample showed a high decomposition temperature ($T_d = 325\ ^\circ C$), revealing the high thermal stability of that lithium ion battery promising sample.

Acknowledgment

The first author of this manuscript would like to thank both of Benha University (http://www.bu.edu.eg/en/) (Project code: 4/1/C; Third stage; N. 10) and the Academy of Scientific Research and Technology (ASRT) (http://www.asrt.sci.eg/) (Graduation project; N. 2; 2014–2015), Egypt, for the financial support of this scientific research work through competitive research projects.

References

[1] A.M. Stephan, Eur. Polym. J. 42 (2006) 21–42.
[2] B. Scrosati, J. Hassoun, Y.-K. Sun, Energy Environ. Sci. 4 (2011) 3287–3295.
[3] H.S. Kim, P. Periasamy, S.I. Moon, J. Power Sources 141 (2005) 293–297.
[4] L.N. Sim, S.R. Majid, A.K. Arof, Vibrat. Spectr. 58 (2012) 57.
[5] D.-W. Kim, K.A. Noh, J.-H. Chun, S.-H. Kim, J.-M. Ko, Solid State Ion. 144 (3–4) (2001) 329.
[6] V. Aravindan, P. Vickraman, A. Sivashanmugam, R. Thirunakaran, S. Gopukumar, Curr. Appl. Phys. 13 (1) (2013) 293.
[7] R. Miao, B. Liu, Z. Zhu, Y. Liu, J. Li, X. Wang, Q. Li, J. Power Sources 184 (2) (2008) 420.
[8] Emad M. Masoud, A.-A. Elbellihi, W.A. Bayoumy, M.A. Mousa, Alloy. Compd. 575 (2013) 223–228.
[9] E.M. Masoud, A.-A. El-Bellihi, W.A. Bayoumy, M.A. Mousa, Mater. Res. Bull. 48 (3) (2013) 1148–1154.
[10] Emad M. Masoud, Alloy. Compd. 651 (2015) 157–163.
[11] Abdelhameed Ahmed ElBellihi, Wafaa Abdallah Bayoumy, Emad Mohamed Masoud, Mahmoud Ahmed Mousa, Bull. Korean. Soc. 33 (9) (2012) 2949–2954.
[12] Emad M. Masoud, Polym. Test. 56 (2016) 65–73.
[13] Chih-Hao Tsao, Ping-Lin Kuo, J. Membr. Sci. 489 (2015) 36–42.
[14] P. Martins, A.C. Lopes, S. Lanceros-Mendez, Prog. Polym. Sci. 39 (4) (2014)

683–706.
[15] G. Cheruvally, J.-K. Kim, J.-W. Choi, J.-H. Ahn, Y.-J. Shin, J. Manuel, P. Raghavan, K.-W. Kim, H.-J. Ahn, D.S. Choi, C.E. Song, J. Power Sources 172 (2007) 863–869.
[16] A.M. Stephan, Y. Saito, Solid State Ion. 148 (2002) 475–481.
[17] V. Aravindan, P. Vickraman, Eur. Polym. J. 43 (2007) 5121–5127.
[18] D. Saikia, Y.W. Chen-Yang, Y.T. Chen, Y.K. Li, S.I. Lin, Desalination 234 (2008) 24–32.
[19] A. Manuel Stephen, K.S. Nahm, M.A. Kulandainathan, G. Ravi, J. Wilson, Eur. Polym. J. 42 (2006) 1728–1734.
[20] M.A. Ratner, D.F. Shriver, Chem. Rev. 88 (1) (1988) 109–124.
[21] A. Reddy Polu, H.W. Rhee, J. Ind. Eng. Chem. 37 (2016) 347–353.
[22] G.P. Pandey, R.C. Agrawal, S.A. Hashmi, J. Power Sources 190 (2009) 563–572.
[23] D. Saikia, A. Kumar, Electrochim. Acta 49 (2004) 2581–2589.
[24] Z. Li, G. Su, X. Wang, D. Gaw, Solid State Ion. 176 (2005) 1903.
[25] N.T. KalyanaSundaram, A. Subramania, ElectrochimicaActa 52 (2007) 4987–4993.
[26] J. Liu, X. Huang, J. Duan, H. Ai, P. Tu, Mat. Lett. 59 (2005) 3710.
[27] H.P. Klug, L.E. Alexander, X – Ray Diffraction Procedures, Wiley, New York, 1970.
[28] M. Ulaganathan, R. Nithya, S. Rajendran, S. Raghu, Solid State Ion. 218 (2012) 7–12.
[29] K.G. Kanade, B.B. Kale, R.C. Aiyer, B.K. Das, Mater. Res. Bull. 41 (2006) 590–600.
[30] F. Croce, G.B. Appetecchi, L. Persi, B. Scrosati, Nature 394 (1998) 456.
[31] K.P. Singh, P.N. Gupta, R.P. Singh, J. Polym. Mater 9 (1992) 131.
[32] A. Awadhia, S.K. Patel, S.L. Agrawal, Prog. Cryst. growth character. mater 52 (2006) 61.
[33] H.M. Xiong, X. Zhao, J.S. Chen, J. Phys. Chem. B105 (2001) 10169.
[34] D. Shanmukaraj, G.X. Wang, R. Murugan, H.K. Liu, Phys. Chem. Solids 69 (2008) 243–248.
[35] Emad M. Masoud, M. Khairy, M.A. Mousa, Alloy. Compd. 569 (2013) 150–155.